Topographic control on lava flow paths at Mt. Etna (Italy): implications for hazard assessment

Massimiliano Favalli[1], Francesco Mazzarini[1], Maria Teresa Pareschi[1], Enzo Boschi[1]
1- Istituto Nazionale di Geofisica e Vulcanologia, Pisa, Italy

Abstract

Assessment of the hazard from lava flow inundation at the active volcano of Mt. Etna (Italy) was performed by calculating the probability of lava flow inundation at each position on the volcano. A probability distribution for the formation of new vents was calculated using geological and volcanological data from past eruptions. The simulated lava flows from these vents were emplaced using a maximum expected flow length derived from geological data on previous lava flows. Simulations were run using DOWNFLOW, a DEM-based model designed to predict lava flow paths. Different eruptive scenarios were simulated by varying the elevation and probability distribution of eruptive points. Inundation maps show that the city of Catania and the coastal zone may only be impacted by flows erupted from low-altitude vents (< 1500 m elevation), and that flank eruptions at elevations > 2000 m preferentially inundate the northeast and southern sectors of the volcano as well as the Valle del Bove. Eruptions occurring in the summit area (> 3000 m elevation) pose no threat to the local population. Discrepancies between the results of simple, hydrological models and those of the DOWNFLOW model show that hydrological approaches are inappropriate when dealing with Etnean lava flows. Because hydrological approaches are not designed to reproduce the full complexity of lava flow spreading, they underestimate the catchment basins when the fluid has a complex rheology.

1. Introduction

The flanks of several basaltic volcanoes are highly populated, and the towns, cities and associated infrastructures may be impacted by lava flows during effusive eruptions. Lava flow hazards on the flanks of such volcanoes (e.g., Mauna Loa, Mt. Etna) are of great concern for the

protection of civilians because of the frequent eruptions and the growing vulnerable population [e.g. Trusdell 1995; Rowland et al., 2005]. It is difficult to assess lava hazard through computer simulations of lava flow [e.g. Crisci et al., 2004a] because of the evolving topography during an eruption: as new lava flows are emplaced, they produce new topographic features that can influence the paths of subsequent lava flows. Lava flows are unconfined, multiphase and multicomponent flows in which temperature, rheology and effusion rates all vary in time and space. Given the high complexity of these processes, in most real case applications it would be impractical to perform a direct numerical simulation of the complete set of flow conservation laws. Because the real-time forecast of lava flow paths is essential during volcanic crises, a number of "simplified" models have been developed; these models are mainly based on the assumption that lava follows the steepest gradient downhill and spreads laterally according to its critical thickness and mass conservation [e.g. Wadge et al., 1994]. Other models are based on a probabilistic definition of lava flow spreading [e.g. Favalli et al., 2005]; they generally involve low CPU execution times and do not require accurate specification of the physical properties of lava (e.g. flow rate, temperature, cristallinity, viscosity, yield strength). Other models are based on cellular automata or neural network approaches [e.g. Crisci et al., 2004a] or on various simplifications of the governing physical equations [e.g. Dragoni et al., 1986; Harris and Rowland, 2001; Costa and Macedonio, 2005].

Here we use a modified version of DOWNFLOW [Favalli et al., 2005]. The previous versions of the DOWNFLOW code [Favalli et al., 2005; Favalli et al., 2006] predicted which areas would be inundated by lava flows erupting from a single vent. The new DOWNFLOW version adopts probability distributions for vent opening and lava flow length distributions to create maps of lava inundation probability.

We applied this new model to lava flow hazard assessment on Mt. Etna volcano, located on the East coast of Sicily (Italy). Mt. Etna is characterized by numerous (near yearly) eruptions accompanied by effusive and moderate explosive activity [Behncke and Neri, 2003; Neri and

Acocella, 2006; Allard et al., 2006]. Eruptions from both summit and flank vents at variable effusion rates have produced numerous composite lava fields [e.g. Harris et al., 2000; Branca and Del Carlo, 2004; Calvari and Pinkerton, 1998; Romano and Sturiale, 1982]. Much of the erupted lava has flowed into a deep scar resulting from flank instability on the eastern flank of the volcano (Valle del Bove) [Borgia et al., 1992].

Existing hazard zonation maps of Etna have been compiled considering the main volcanological parameters of all eruptions since A.D. 1600 (e.g., including vent location, age, type of eruption, volume of lava flow and tephra) and the areas invaded by lava flows since 700 B.C.; they assume that the characteristics of future eruptions will be similar to those of past eruptions [Guest and Murray, 1979; Andronico and Lodato, 2005; Behncke et al., 2005]. We propose a different hazard assessment approach based not only on the frequency of coverage of past lava flows, but also on the numerical simulation of possible lava flow paths, taking into account the actual topography over which lavas flow. Updated high resolution digital elevation models (DEM) of Mt. Etna have recently been derived from LiDAR (Light Detection and Ranging) data [Mazzarini et al., 2005; 2007]. Using vent and lava flow length distributions based on the statistical analysis of past eruptions, DOWNFLOW performs simulations of all possible future lava flow paths and produces detailed quantitative maps of the probability of inundation by lava flows. This is possible because: i) DOWNFLOW accounts for the most relevant emplacement characteristics of real lava flows, such as filling of topographic depressions, overriding of topographic obstacles and lava flow spreading, without requiring detailed input parameters; ii) the code is able to compute invasion areas from each vent in a very short computational time; iii) simulation outputs require relatively little disk space. Lava flow paths from all possible vents can therefore easily be simulated and stored, results can be post-processed to produce quantitative hazard maps for different scenarios, and lava catchment areas can be identified rigorously by considering all the vents from which lava flows can invade a target area.

2. Mt. Etna Digital Elevation Model

Airborne altimetric LiDAR data were used to generate a high-resolution (2 m) DEM of most of Mt. Etna from data acquired during flights on September 29 (8:00-11:00 a.m. local time) and September 30 (8:00-10:30 a.m. local time) 2005. LiDAR data have already proved useful in analyzing the morphology of rapidly evolving features of the landscape, for example active volcanoes [e.g. Mazzarini et al., 2005; Mazzarini et al., 2007; Ventura and Vilardo, 2007], as well as in lava flow modeling [e.g. Harris et al., 2007].

An ALTM 3033 (Optech®) laser altimeter (see Table 1 for instrument characteristics) was used to survey an area of 616 km^2. Measurements were made at a frequency of 33 kHz, resulting in a mean ground point density of 1 point per 2.4 m^2 (generally one point every 1.5 x 1.5 m^2). The LiDAR survey consists of more than 2.57 x 10^8 data points. These points (echoes) were distributed along 34 NNE-SSW trending strips covering part of Etna's western flanks and the majority of its eastern flanks. The resulting DEM, geocoded to a UTM-WGS 84 projection, has an elevation accuracy of ±0.4 m and a horizontal accuracy of ±1.5 m.

At the LiDAR operating wavelength (λ = 1.064 μm), atmospheric absorption is minimum; however, during an eruption, ash and gases can greatly hamper data acquisition. Likewise, persistent degassing such as that which feeds a constant plume at Etna can cause unwanted atmospheric effects, especially near the summit craters. Our September 2005 LiDAR survey (with flight altitudes ranging from 1500 to 3500 m) occurred during a period of low volcanic activity characterized by clear atmospheric conditions. A 10 m step DEM was derived from the LiDAR data. Outside the region covered by the LiDAR survey, the LiDAR DEM was merged with a 10 m step DEM of all of Italy created by Tarquini et al. [2007].

3 Lava flow simulation

3.1 The DOWNFLOW probabilistic code

DOWNFLOW [Favalli et al., 2005] computes maximum slope paths on a stochastically perturbed topography. It is based on an assessment of the steepest descent path, which is derived multiple times (generally thousands of times) on a randomly perturbed topography in an attempt to quantify all possible flow paths. For each emission point, only two model parameters must be input. The first parameter (Δh) represents the maximum vertical perturbation (either positive or negative) which is applied to the DEM during each iteration. The second parameter (n) represents the number of steepest descent path calculations performed for any single run from a user-defined emission point [Favalli et al., 2005; 2006].

Favalli et al. [2005] performed a dimensional analysis of steady-state lava flows on an inclined plane; results indicated that lava spreading is controlled by the competing viscous and gravitational/ self-gravitational (hydrostatic) forces. These forces can be characterized by a vertical scale length H that approximates the size of obstacles which can be overridden by the flow. Stochastic variations in ground elevation by a characteristic vertical height equal to $2\Delta h \cong H$ employed in the computation of maximum slope paths therefore account for first-order variations in lava flow spreading. An appropriate value of Δh can be obtained through the best fit of simulated and actual lava flows; such a value relates to the characteristic height of obstacles capable of diverging the flow. In the case of Mt. Etna, the best fit to lava flow maps for the 1991-1993, 2001 and 2002 flank eruptions is given by Δh = 3 m and n = 10,000 [Favalli et al., 2005]. For example, the simulated inundation area of the 2001 flow covers 90% of the actual flow. We thus assume that these Δh and n values are appropriate for typical flank eruptions at Etna. Comparison between real and simulated flow fields at Etna and Nyiragongo indicates that the DOWNFLOW approach yields realistic emplacement areas [Favalli et al., 2005; 2006].

We applied DOWNFLOW to Mt. Etna, for which a high resolution LIDAR-derived DEM is available. We checked the sensitivity of DOWNFLOW against the DEM resolution in the case of the southern 2001 lava flow at Mt. Etna [Favalli et al., 2005]. The 1998 DEM of Tarquini et al. [2007], with a cell size of 10m, was used as a topographic base. The DEM root mean square (RMS)

vertical error in the study area is 1.43 m. By resampling the original DEM, we generated a series of new DEMs with different cell sizes (up to 120 m) and vertical errors (up to 4.23 m), as reported in Table 2. We then performed simulations with DOWNFLOW for each newly generated DEM, using the 2001 vent as the starting point, with Δh = 3 m and n = 10,000. To compare the simulations with the actual flow, for each simulation we calculated the parameter μ:

$$\mu = \frac{A_S \cap A_R}{A_S \cup A_R}$$

where A_S is the area covered by our simulation and A_R is the area covered by the actual 2001 flow; μ is 1 when these two areas coincide. In the case of the 10-m DEM we obtained a μ value of 0.52, which indicates that there is good agreement between the simulated flow and the actual flow. As shown in Table 2, the agreement between the simulated flow and the actual 2001 lava flow is almost constant up to grid cells of 90 m (or up to RMS vertical errors of 3.27 m), whereas μ values gently decrease for higher cell dimensions. The probabilistic nature of DOWNFLOW is such that intrinsic errors in the adopted DEM are overcome, since random perturbations of the topography already add random 'errors' to the topography.

Recently DOWNFLOW was applied on DEMs of coarser resolution. In particular, DOWNFLOW has successfully reproduced the 1977 and 2002 lava flows at Nyiragongo Volcano using a 90-m pixel DEM derived from the Shuttle Radar Topographic Mission (SRTM; http://www2.jpl.nasa.gov/srtm) as a topographic base [Favalli et al., 2008]. This indicates that DOWNFLOW can be used with the SRTM digital elevation model for most volcanoes in the world where high resolution data are not yet available.

However, the model allows neither a description of the time evolution of lava flows and of the effects of effusion rates, nor the definition of flow lengths. Accordingly, the length distribution for the simulated lava flow must be input.

3.2 Probability distribution of vents

158 Although eruptions at Mt. Etna occur from both the summit and flanks, we focus on the hazard
159 due to flank eruptions, which have proved to be the most dangerous in the past [Chester et al., 1985;
160 Mulargia et al., 1985; Crisci et al., 2004b; Andronico and Lodato, 2005; Behncke et al., 2005] and
161 often have the highest effusion rates [Harris et al., 2000; Wadge 1981]. According to Guest and
162 Murray [1979] and Chester et al. [1985], certain flank areas of Mt. Etna are more likely to produce
163 eruptions than others; these areas correspond to zones with a high density of cones and eruptive
164 fractures, i.e. the NE, S and W rift zones [e.g. Kieffer, 1975].
165 The probability of a vent opening in a certain location is usually based on the assumption that
166 future vents will form in zones with the highest density of old vents [Guest and Murray, 1979;
167 Behncke et al., 2005]. The location of more than 400 vents were thus extracted from LiDAR-based
168 DEMs of Mt. Etna and published maps [Mazzarini and Armienti, 2001]. From this discrete set of
169 points we estimated the vent opening probability distribution through a kernel smoothing technique
170 [Bowman and Azzalini, 2003] using a Gaussian kernel with a bandwidth of 1 km. In Fig. 1 we plot
171 the smoothing kernel over the vent spacing distribution. The distribution of vent spacing (vent
172 separation) was calculated by computing the distance between each vent and the nearest neighbor
173 vent. Results show that there is a very low probability that a vent will open less than 80 m from
174 another vent. The probability distribution for vent opening was thus assessed using the vent density
175 map and the 80 m proximity threshold (Fig. 2). This vent opening distribution does not, of course,
176 take into account the possibility of vents or vent clusters opening in areas where vents are currently
177 not exposed at the surface. This possibility is taken into account, as described in the following
178 sections, by using a uniform vent distribution.
179
180 **3.3 Lava flow length distribution**
181 Following Favalli et al. [2005], data from Guest [1982], Behncke et al. [2005], Allard et al.
182 [2006], and Neri and Acocella [2006] was plotted on a flow length versus vent elevation diagram

(Fig. 3). In the last two decades eruptions have occurred above 2000 m and have been characterized by a maximum runout distance of 8.75 km [Behncke et al., 2005].

According to Guest [1982] and Lopes and Guest [1982], at Mt. Etna there is an inverse correlation between vent elevation (h_v) and the length of the erupted lava flow (L): the lower the elevation the longer the lava flow. The points in the h_v-L space for the lava flows at Mt. Etna (Fig. 3) are bounded by a straight line defined by the following equation [Favalli et al., 2005]:

$$L_l = -6.25\, h_v + 26{,}075 \quad (1)$$

where h_v (m) is the vent elevation and L_l (m) is the maximum runout distance of the lava flow front.

For our purposes, we need to know the probability PL_{ij} that a lava flow originating from a given location i reaches a site j. We thus assume $PL_{ij} = 0$ if the distance along the flow path from vent i to site j (L_{ij}) is greater than L_l, as defined in equation (1); $PL_{ij} = 1$ when $L_{ij} \leq 0.5L_l$, and it increases linearly from 0 to 1 when $L_l > L_{ij} > 0.5L_l$. Equation (1) gives the maximum runout distance for lava flows erupting at a given elevation. It actually overestimates maximum lava flow lengths for vents at altitudes < 2000 m. For example, using equation (1), the maximum length of lava flows erupted at an elevation of 1500 m is 16,700 m. To quantify the impact of length overestimation on the final probability maps, let us assume that the real length of lava flows erupted at 1500 m is 14,000 m instead of 16,700 m. This would produce a variation of only 2% in the probabilities of inundation in the final hazard map.

4. Maps of the probability of lava inundation

Maps of the probability of inundation by lava flows were compiled for Mt. Etna using DOWNFLOW [Favalli et al., 2005]. The maps represent the probability that a given location will be inundated by lava flows in the case of a flank eruption. The inundation probability maps are based on: (i) the probability distribution of future vents (PV), and (ii) the probability length distribution of future lava flows (PL).

The probability of inundation (P_j) by lava flows at a generic site *j* is defined as:

$$P_j = \Sigma_i \, PV_i \times PS_{ij} \times PL_{ij} \quad (2)$$

where the sum is over all the vents *i*, PV_i is the probability that a vent forms at location *i*, PS_{ij} is the probability that site *j* is inundated by a lava flow erupted from a vent at location *i* (using the DOWNFLOW simulation code), and PL_{ij} is the probability that a lava flow originating from location *i* has the capability to reach site *j*, as defined in the previous section.

The 10 meter DEM was used as a computational grid for the simulations. The selected vent or source region includes all areas with a vent opening probability higher than 0.1 %/km^2, for a total surface area of 320 km^2. Computational vents were chosen on a regular mesh with a node separation of 80 m.

To test the influence of the initial vent distribution, several inundation maps were prepared (Figs. 4 to 7). The maps were compiled on the basis of 5 x 10^4 simulations, i.e. simulations were run from 5 x 10^4 likely vent locations, which allowed the computation of a total of 5 x 10^8 lava flow paths. Each of these simulations took a few minutes. The vent probability threshold (0.1 %/km^2) was used to obtain an acceptable compromise between CPU time and the accuracy of the final inundation maps. The inclusion of regions with vent opening probabilities lower than 0.1 %/km^2 contributes negligibly to the final maps but increases the computational time by more then 100 days.

Using the total vent probability distribution as a source region (Fig. 2), the highest inundation probabilities are in the south-southeastern, western, and northeastern sectors, at elevations below 1500 m above sea level (Fig. 4). The longest lava flows are able to impact Catania and the coastal areas; these flows originate from source vents located in two main areas, one at an elevation of about 1500 m and the other at about 800 m. Comparison of Fig. 4 with Fig. 3 in Guest and Murray [1979] reveals that the main advantage of our approach is that it allows the quantification of hazard (inundation probability): the Guest and Murray [1979] approach cannot be used to identify regions most prone to inundation by lava flows, whereas their identification is straightforward in Fig. 4.

Based on the steepest descent paths, Guest and Murray [1979] produced maps of the maximum extent of lava flows erupted from the outer edge of the region with a probability of vent opening > 1 vent per km^2. A comparison of their maps with our probability maps for venting above 2000 m is shown in Fig. 8 for the northern sector of the volcano. In comparing these maps, we must consider the different accuracy of the two different topographic bases (i.e. our 2 m LIDAR DEM versus 25 m contour topographic maps) and the time interval between the two (about 30 years of volcanic activity). The map by Guest and Murray [1979] only qualitatively displays the lava paths and does not specify the probability that any given point along a path will be invaded by lava. For example, based on our maps, zones a and b in Fig. 8 have very different probabilities of invasion (0.2% and 12%, respectively), whereas no probability estimate is provided in the map by Guest and Murray [1979]. Even if we consider the density of steepest descent paths as a rough indicator of the probability of invasion in Guest and Murray [1979], areas with very high path densities in their map correspond to areas with low lava flow invasion probability in Fig 8 (e.g., zone c). Moreover, Guest and Murray's [1979] map was derived specifying vents only on the outer edge of the region having a probability of vent opening greater than 1 vent per km^2 and not considering the actual spatial distribution of the vent opening probability, i.e. neglecting the contribution of vents inside the 1 vent per km^2 contour (e.g., Fig. 2 of Guest and Murray [1979]).

In the last decade, flank activity at Mt. Etna has been characterized by eruptions from vents located at elevations above 2000 m [e.g. Andronico and Lodato, 2005]. Accordingly, an inundation probability map was compiled considering the possibility of new vents opening above an elevation of 2000 m only (Fig. 5). The resulting map shows the highest inundation probability in areas where lava flows have been emplaced recently (Figs. 5, 9 and 10). With the 2000 m vent elevation threshold, the zones with the highest probability move uphill due to the higher elevation of the starting positions and the maximum length condition imposed by equation 1 (Fig. 5).

To highlight the low hazard in the case of vent opening in the summit region, a map was produced assuming a uniform vent distribution for vents located above an elevation of 3000 m. For

eruptions from vents located above 3000 m, the inundation region is limited to a distance of about 7 km from the summit (Fig. 6), extending downhill to an elevation of 1500 m, thereby posing no threat of lava flow inundation to inhabited areas. The rims of the Valle del Bove (VDB in Fig. 2) clearly protect portions of the flank from summit eruptions, which are contained within the valley. Moreover, the 2002-2003 cones and lava field play a role in controlling the path of simulated lava flows: the newly formed volcanic constructs hinder the southward propagation of simulated lava flows (Fig. 6).

Lava flows modify the landscape, generating new morphologies that may or may not hinder the path of future flows. This process is evident from the fields emplaced during the 2001 and 2002-2003 Mt. Etna eruptions. In the case of the southern 2001 eruption (Fig. 9), the highest probability of inundation is mainly attained along a strip parallel to the 2001 flow, and the thick 2001 flow front has a near-zero probability of inundation because it is now a topographic high. In contrast, the 2002-2003 flow (Fig. 10) was emplaced in a valley with a high probability of inundation, and future flows will thus pile up on the 2002-2003 flow.

All the presented maps are based on the 2005 topography. During July-November 2006, a new summit eruption occurred that produced two main lava flows: a southwest flow and an easterly flow (http://www.ct.ingv.it/Etna2006/Default.htm). We used this eruption to check the accuracy of our methodology. The probability map of flow inundation for a uniform vent distribution across the summit zone (i.e. above an elevation of 3000 m) was compared with the actual flows erupted in 2006 (Fig. 11). The use of a uniform vent distribution does not completely account for the actual vent distribution in the summit zone. For example, it underestimates the relevance of the small area occupied by the SE Crater (SEC), which has been the principal site of effusive eruptions in the last few years [Allard et al. 2006]. According to Fig. 6, this frequently inundated region downstream of the SEC has low inundation probability values. This incongruity relates to the use of a uniform vent distribution; the inundation probability values depend on the extent of the area where vents may open: the larger the area, the higher the probability.

The area covered by the southwest lava flow, erupted from a fissure located on the southern flank of the summit crater (Fig. 11), matches well with the predicted high probability zone in Figs. 6 and 10. The eastern lava flow (Fig. 11) erupted from the base of the SEC covers a medium-probability (3-8%) zone; at the end of its path it enters the high-probability (8-16%) area supplied by lava from the entire summit crater.

To highlight the importance of vent distribution, a map of the probability of inundation was produced considering the possible opening of new vents above an elevation of 2000 m only and assuming a uniform vent distribution (Fig. 7). The overall symmetry of the volcano's edifice results in an almost symmetrical distribution of inundation probabilities. Deviations from this general pattern occur in the principal basins. For example, concavities in the 2000 m contour tend to focus flow paths towards the center of each concavity, resulting in high inundation probabilities downslope of such topographic features (Fig. 7). Comparison of the probability maps generated using non-uniform (Fig. 5) and uniform (Fig. 7) vent distributions and considering the possible opening of vents above 2000 m only reveals that the non-uniform simulation better accounts for the effusive activity of the last 10 years. This is evident when comparing the probability maps with the map of real lava flows at Mt. Etna from 1995 to 2005 (Fig. 1 in Allard et al., [2006]).

These probability maps give the spatial probability of inundation for the opening of a new vent. We next considered the probability $p_{erupt}(x,t)$ that, in a given time interval (t), a given location (x) would be inundated by lava. To do this, we combined (1) the probability $p_{erupt}(t)$ that at least one eruption would occur during time t with (2) the probability $p_{in}(x)$ that each eruption would inundate a given location. Figs. 4 to 7 display $p_{in}(x)$ values for each vent distribution scenario considered herein.

Assuming that eruptions are randomly distributed in time and have an average recurrence interval (T), following Kauahikaua et al. [1995] we used a Poisson distribution to estimate the probability that at least one eruption would occur within time t:

$$p_{erupt}(t) = \sum_{n=1}^{+\infty} p_n(t) = 1 - e^{-\frac{t}{T}} \quad (3)$$

in which

$$p_n(t) = \frac{1}{n!}\left(\frac{t}{T}\right)^n e^{-\frac{t}{T}} \quad (4)$$

where this is the probability of the occurrence of n lava flows within time t, and $e^{-t/T}$ is the probability that no eruptions would occur in time interval t. The probability that at least one eruption would inundate a given location therefore becomes:

$$p_{erupt}(x,t) = \sum_{n=1}^{+\infty} p_n(t) \cdot \left[1 - (1 - p_{in}(x))^n\right] = 1 - e^{-\frac{t}{T} p_{in}(x)} \quad (5)$$

where the term within the square brackets represents the probability that at least one of n lava flows would inundate location x.

As an example, we calculated the probability that the zone invaded by the eastern 2002-2003 flow (Fig. 10) would be inundated again within the next year. The spatial inundation probability $p_{in}(x)$ for the 2002-2003 inundation zones is 15% (Fig. 10). During 1989 – 2006, there were 8 flank eruptions [Behncke et al., 2005], all from vents above 2000 m and with an average recurrence time of 2.2 years (i.e., 17 years divided by 8 eruptions). By applying equation (3), the probability of a flank eruption in the next year is 37%. Based on equation (5), the probability $p_{erupt}(x,t)$ that the zone invaded by the 2002-2003 eastern flow would be invaded again in the next year is 6.8%.

5. Lava catchments

For hazard management purposes it is important to identify areas able to produce lava flows that can potentially invade populated areas. Guest and Murray [1979] and Kauahikaua et al. [1995] used catchment area and watershed (or lava-shed) methods to estimate lava flow hazard at Mt. Etna and Mauna Loa, respectively. The use of a simple hydrological catchment-based approach to identify source areas that could generate flows capable of inundating a given location is not appropriate for

lava flows. Lava flows are generally some meters thick: they can thus spread out and override obstacles. Lava flows do not necessarily follow the maximum slope path, but can split into different branches and form complex patterns. DOWNFLOW provides realistic emplacement areas, whereas a single maximum slope path (which is the basic element in building hydrological catchment areas) does not account for the actual extent of lava flows, e.g. as in the case of the 2001 south flank lava flow (Fig. 9).

Our simulation-derived database allows the identification of all simulated flows that are able to inundate a selected city, town or village. By identifying those vents from which simulated lava flows are capable of reaching a given region (e.g., a village), we can create a map of areas posing a threat to the region (lava catchments).

In Fig. 12, selected lava catchments (colored areas) are compared to the corresponding hydrologically-derived catchments (black lines) for selected villages (brown areas). The computed lava catchments were divided into three different subregions according to the length of the lava path required to reach the villages. Catchments areas in Fig. 12 are thus color-coded according to the three main regions in the elevation-length plot (Fig. 3). The cyan region in Fig. 12 corresponds to source areas for which the length of the simulated lava flows is always shorter than the distance between vent and village, i.e. the flow cannot reach the village. The orange region on Fig. 12 produces lava flows that, according to the simulations, are always able to reach the villages. The yellow region represents source areas in which the probability that the simulated flow would reach the village is between 0 and 1.

We note that lava-sheds generated by the hydrological approach may account for only minor portions of those generated by the DOWNFLOW approach. Previous hydrological approaches (e.g. see Fig. 6 of Guest and Murray, 1979) generally underestimate the hazard by lava flow inundation. For example, in the case of the town of Nicolosi the hydrologically-derived area is about one quarter of that obtained using the DOWNFLOW-based approach (Fig. 12).

6. Conclusions

The DOWNFLOW topography-based stochastic model requires very short computational times and is as effective as more sophisticated physical models in assessing lava flow hazard. DOWNFLOW does not require the specification of physical quantities such as effusion rates, temperature, crystallinity, viscosity, yield strength, etc., and does not simulate the time evolution of single lava flows. It determines, instead, the total area inundated by lava flows, i.e. an essential parameter for producing hazard maps. Our lava flow hazard maps for Mt. Etna quantitatively define the probability of inundation by lava flows based on a probabilistic approach dependent on the topography, probable opening locations, and likely lava flow run-out distances. The reliability of the proposed method requires the use of updated elevation models of the volcanic area. Simulations were run on a DEM derived from 2005 LiDAR data. Depending on effusion rates and duration, eruptions determine the formation of topographic features that may impede or favor inundation by successive lava flows and our simulations support this.

Different vent opening probability distributions were used to simulate different eruptive scenarios: (a) an unconstrained vent opening distribution (i.e., vents can open at any elevation); (b) vent opening above 2000 m; (c) vent opening above 3000 m; and (d) a uniform distribution of vents opening above 2000 m. Here, (a), (b) and (c) consider a non-uniform vent distribution, whereas (d) assumes a uniform distribution. Based on the analysis of these maps we come to the following conclusions:

1) The city of Catania and the coastal zone are only susceptible to inundation from flows originating from low altitude vents (below 1500 m).

2) Flank eruptions above 2000 m preferentially inundate the northeast and southern sectors of the volcano, as well as the Valle del Bove.

3) Eruptions in the summit area (above 3000 m) pose no threat to populated areas.

4) Simple hydrological approaches based on static topography are inappropriate when dealing with Etnean lava flows. They tend to produce a single, overly simplified path, whereas DOWNFLOW is calibrated to simulate the full complexity of lava flow spreading.

The inundation probability maps provide detailed spatial distributions of the possible lava flow paths and are useful tools in long-term planning and decision-making for mitigation of lava flow inundation hazard. This is a particularly important issue in the case of Mt. Etna because of its high population density and the frequency of eruptions.

Acknowledgments. This work was funded by “Progetto INGV-DPC 2005-2006 – Vulcanologia - Subproject - V3_6 – Etna – UR-31”, scientific coordinator M.T. Pareschi.

References

Allard, P., B. Behncke, S. D'Amico, M. Neri, and S. Gambino (2006), Mount Etna 1993-2005: Anatomy of an evolving eruptive cycle, *Earth Science Reviews*, 78, 85-114.

Andronico, D., and L. Lodato (2005), Effusive activity at Mount Etna volcano (Italy) during the 20th century: a contribution to volcanicn hazard assessment, *Natl Hazards*, 36, 407-443.

Behncke, B. and M. Neri (2003), Cicles and trends in the recent eruptive behaviour of Mount Etna (Italy), *Can. J. Earth Sci.*, 40, 1405-1411

Behncke, B., M. Neri and A. Nagay (2005), Lava flow hazard at Mount Etna (Italy): New data from a GIS-based study, in Kinematics and dynamics of lava flows: Geological Society of America Special Paper, vol. 396, edited by M. Manga, and G. Ventura, pp. 189-208.

Borgia, A., L. Ferrari, and G. Pasquare` (1992), Importance of gravitational spreading in the tectonic and volcanic evolution of Mount Etna, *Nature*, 357, 231– 235.

Bowman, a. W., and A. Azzalini (2003), Computational aspects of nonparametric smoothing with illustrations from the sm library, *Computational Statistics & Data Analysis*, 42, 4, 545-560, doi:10.1016/S0167-9473(02)00118-4.

Branca, S. and P. Del Carlo (2004), Eruptions of Mt. Etna during the past 3200 years: A revised compilation integrating the historical and stratigraphic records, in *Mt. Etna: Volcano Laboratory: Geophys. Monogr. Ser.*, vol. 143, edited by A. Bonaccorso, S.Calvari, M. Coltelli, C. Del Negro and S. Falsaperla, pp. 1-27, AGU Washington, D.C.

Calvari, S., and H. Pinkerton (1998), Formation of lava tubes and extensive flow field during the 1991– 1993 eruption of Mount Etna, *J. Geophys. Res.*, 103, 27,291– 27,301.

Chester, D.K., A.M. Duncan, J.E. Guest and C.R.J. Kilburn (1985), *Mount Etna the anatomy of a volcano*, 404 pp., Chapman and Hall, London.

Costa, A., and G. Macedonio (2005), Numerical simulation of lava flows based on depth-averaged equations, *Geophys. Res. Lett.*, 32, L05304, doi:10.1029/2004GL021817.

Crisci, G.M., R. Rongo, S. Di Gregorio and W. Spataro (2004a), The simulation model SCIARA: The 1991 and 2001 lava flows a Mt. Etna, *J. Volcanol. and Geotherm. Res.*, 132, 253– 267.

Crisci, G.M., S. Di Gregorio, R. Rongo, M. Scarpelli, W. Spataro and S. Calvari (2004b), Revisiting the 1669 Etnean eruptive crisis using a cellular automata model and implications for the volcanic hazard in the Catania area, *J. Volcanol. and Geotherm. Res.*, 123, 211– 230.

Dragoni, M., M. Bonafede, and E. Boschi (1986), Downslope flow models of a Bingham liquid: Implications for lava flows, *J. Volcanol. Geotherm.* Res., 30, 305– 325.

428 Favalli, M., and M.T. Pareschi (2004), Digital elevation model construction from structured topographic data: The
429 DEST algorithm, *J. Geophys. Res.*, 109, F04004, doi:10.1029/2004JF000150.
430 Favalli, M., M.T. Pareschi, A. Neri and I. Isola (2005), Forecasting lava flow paths by a stochastic approach, *Geophys.*
431 *Res. Lett.*, 32, L03305, doi:10.1029/2004GL021718.
432 Favalli, M., G.D. Chirico, P. Papale, M.T. Pareschi, M. Coltelli, N. Lucaya and E. Boschi (2006), Computer simulations
433 of lava flow paths in the town of Goma, Nyiragongo volcano, Democratic Republic of Congo, *J. Geophys. Res.*,
434 111, B06202, doi:10.1029/2004JB003527.
435 Favalli, M., G.D. Chirico, P. Papale, M.T. Pareschi and E. Boschi (2008) Lava flow hazard at Nyiragongo volcano,
436 D.R.C. 1. Model calibration and hazard mapping. *Bull Volcanol*, DOI 10.1007/s00445-008-0233-y.
437 Guest, J.E., and J.B. Murray (1979), An analysis of hazard from Mount Etna volcano, *Journal of the Geological Society*
438 *of London*, 136, 347-354.
439 Guest, J. E., (1982), Styles of eruption and flow morphology on Mount Etna, in Romano, R., ed., Mt. Etna Volcano: A
440 Review of the Recent Earth Science Studies, Memorie della Società Geologica Italiana, 23, 49– 73.
441 Harris, A.J.L., and S.K. Rowland (2001), FLOWGO: A kinematic thermo-rheological model for lava flowing in a
442 channel, *Bull. Volcanol.*, 63, 20-44, doi:10.1007/s004450000120.
443 Harris, A.J.L., J.B. Murray, S.E. Aries, M.A. Davies, L.P. Flynn, M.J. Wooster, R. Wright and D.A. Rothery (2000),
444 Effusion rate trends at Etna and Krafla and their implications for eruptive mechanisms, *J. Volcanol. Geotherm. Res.*
445 102, 237–270
446 Harris, A., M. Favalli, F. Mazzarini, and M. T. Pareschi (2007), Best-fit results from application of a thermo-rheological
447 model for channelized lava flow to high spatial resolution morphological data, *Geophys. Res. Lett.*, 34, L01301,
448 doi:10.1029/2006GL028126.
449 Kauahikaua, J., S. Margriter, J. Lockwood and F. Trusdell (1995), Applications of GIS to the estimation of lava flow
450 hazard on Mauna Loa Volcano, Hawai'I, AGU Geophys Monogr, 92, 315-125.
451 Kieffer, G., (1975), Sur l'existence d'une "riftzone" à l'Etna, Comptes Rendus de l'Académie des Sciences Paris, ser.
452 D, 280, 263-266.
453 Lopes, R., and J.E. Guest (1982), Lava flows on Etna, a morphometric study, in: The Comparative Study of Planets,
454 D.Reidel, Holland.
455 Mazzarini, F., and P. Armienti (2001), Flank cones at Mount Etna volcano; Do they have a power-law distribution, *Bull.*
456 *Volcanol.*, 62, 420-430.

Mazzarini, F., M. T. Pareschi, M. Favalli, I. Isola, S. Tarquini, and E. Boschi (2005), Morphology of basaltic lava channels during the Mt. Etna September 2004 eruption from airborne laser altimeter data, *Geophys. Res. Lett*., 32, L04305, doi:10.1029/2004GL021815.

Mazzarini, F., M. T. Pareschi, M. Favalli, I. Isola, S. Tarquini, and E. Boschi (2007), Lava flow identification and aging by means of lidar intensity: Mount Etna case, *J. Geophys. Res*., 112, B02201, doi:10.1029/2005JB004166.

Mulargia, F., S Tinti and E. Boschi (1985), A Statistical-Analysis of Flank Eruptions on Etna Volcano, *J. Volcanol. Geotherm. Res.*, 23 (3-4), .

Neri, M., and V. Acocella (2006), The 2004-2005 Etna eruption: Implications for flank deformation and structural behaviour of the volcano, *J. Volcanol. and Geotherm. Res.*, 158, 195-206.

Romano, R., and C. Sturiale (1982), The historical eruptions of Mt. Etna (Volcanological data), Memorie della Società Geologica Italiana, 23, 75-97.

Rowland, S.K., H. Garbeil and A.J.L. Harris (2005), Lengths and hazards from channel-fed lava flows on Mauna Loa, Hawai'I, determined from thermal and downslope modeling with FLOWGO, *Bull Volcanol*, 67, 634-647, doi:10.1007/s00445-004-0399-x.

Tarquini, S., I. Isola, M. Favalli, F. Mazzarini, M. Bisson, M. T. Pareschi and E. Boschi (2007),TINITALY/01: a new Triangular Irregular Network of Italy, Annals of Geophysics, 50, 3, in press.

Trusdell, F.A .,(1995) Lava flow hazards and risk assessment on Mauna Loa Volcano, Hawai'I, AGU Geophys Monogr 92, 327–336

Ventura, G., and G. Vilardo (2007), Emplacement mechanism of gravity flows inferred from high resolution Lidar data: The 1944 Somma–Vesuvius lava flow (Italy), *Geomorphology*, doi:10.1016/j.geomorph.2007.06.005

Wadge, G., (1981), The variation of magma discharge during basaltic eruptions. *J. Volcanol. Geotherm. Res.* ,11, 139–168.

Wadge, G., P.A.V. Young and I..J. McKendrick (1994), Mapping lava flow hazard using computer simulation, *J. Geophys. Res.*, 99, 489– 504.

481 Table 1. ALTM 3033 (Optech®) laser altimeter characteristics.

482

Operating scan frequency	33 kHz up to 40 kHz
Operating altitude	80 to 3500 m
Maximum scan angle	± 40°
Horizontal accuracy	1/2000 x altitude at 1 sigma
Elevation accuracy	± 15 cm at 1.2 km and ± 35 cm at 3000 m at 1 sigma
Operating wavelength	1.064 μm

483

484

485 Table 2. RMS vertical error and measure (μ) of the agreement between simulated and actual lava

486 flows for various grid steps in the case of the 2001 southern lava flow.

487

Grid step (m)	RMS vertical error (m)	μ
10	1.43	0.52
20	1.59	0.53
30	1.74	0.52
40	1.97	0.51
50	2.22	0.46
60	2.53	0.49
70	2.84	0.44
80	3.13	0.51
90	3.37	0.48
100	3.68	0.42
110	4.03	0.33
120	4.23	0.26

Figure Captions

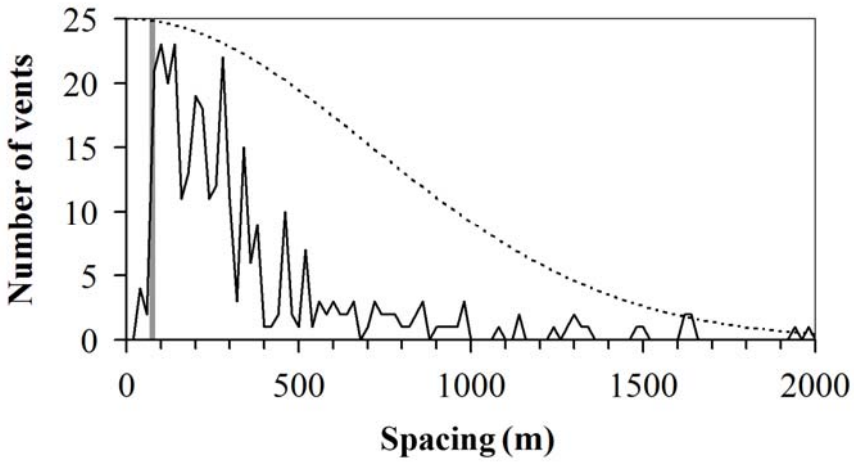

Fig. 1. Plot of the vent spacing distribution. The thick black line is the frequency distribution of vent spacing. The 80 m threshold used to locate new vents is represented as a thick vertical grey line. The dashed line is the smoothing Gaussian kernel used to derive the vent opening probability distribution.

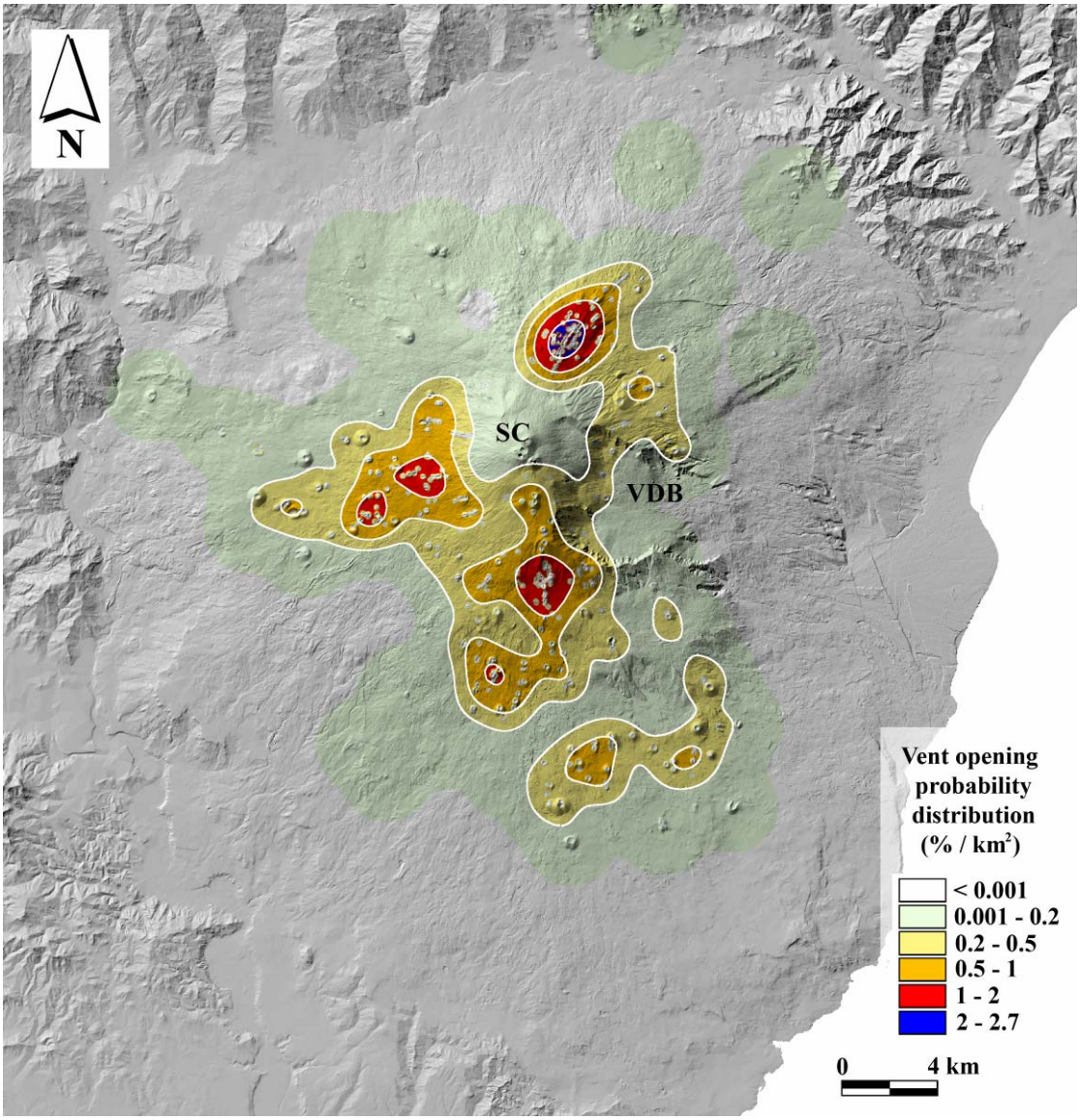

Fig. 2. Map of the vent opening probability used in equation 2 (see text) to estimate the probability (PV_i) of vent formation at location *i*.

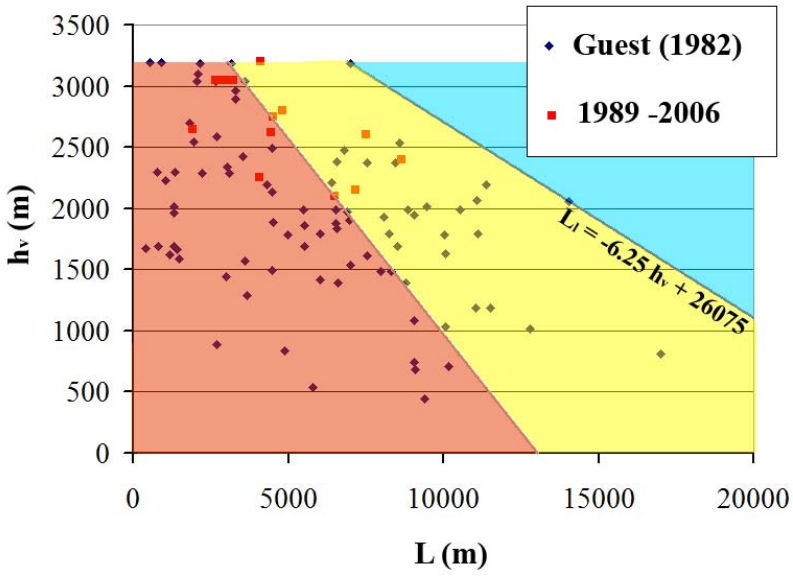

Fig. 3. Plot of lava flow length (L) vs. vent elevation (h_v) for Mt. Etna (black diamonds after Guest, 1982). The orange color in the plot represents the zone in which the flow length is $\leq 0.5L_l$, where L_l is derived from equation 1 in the main text. In the yellow zone the length of flows is in the $0.5L_l < L < L_l$ range. The cyan color represents zones in which the flow length is $\geq L_l$. Red squares in the plot are derived from new digital elevation models of the volcano and from data in Behncke et al. (2005), Allard et al., (2006) and Neri and Acocella (2006).

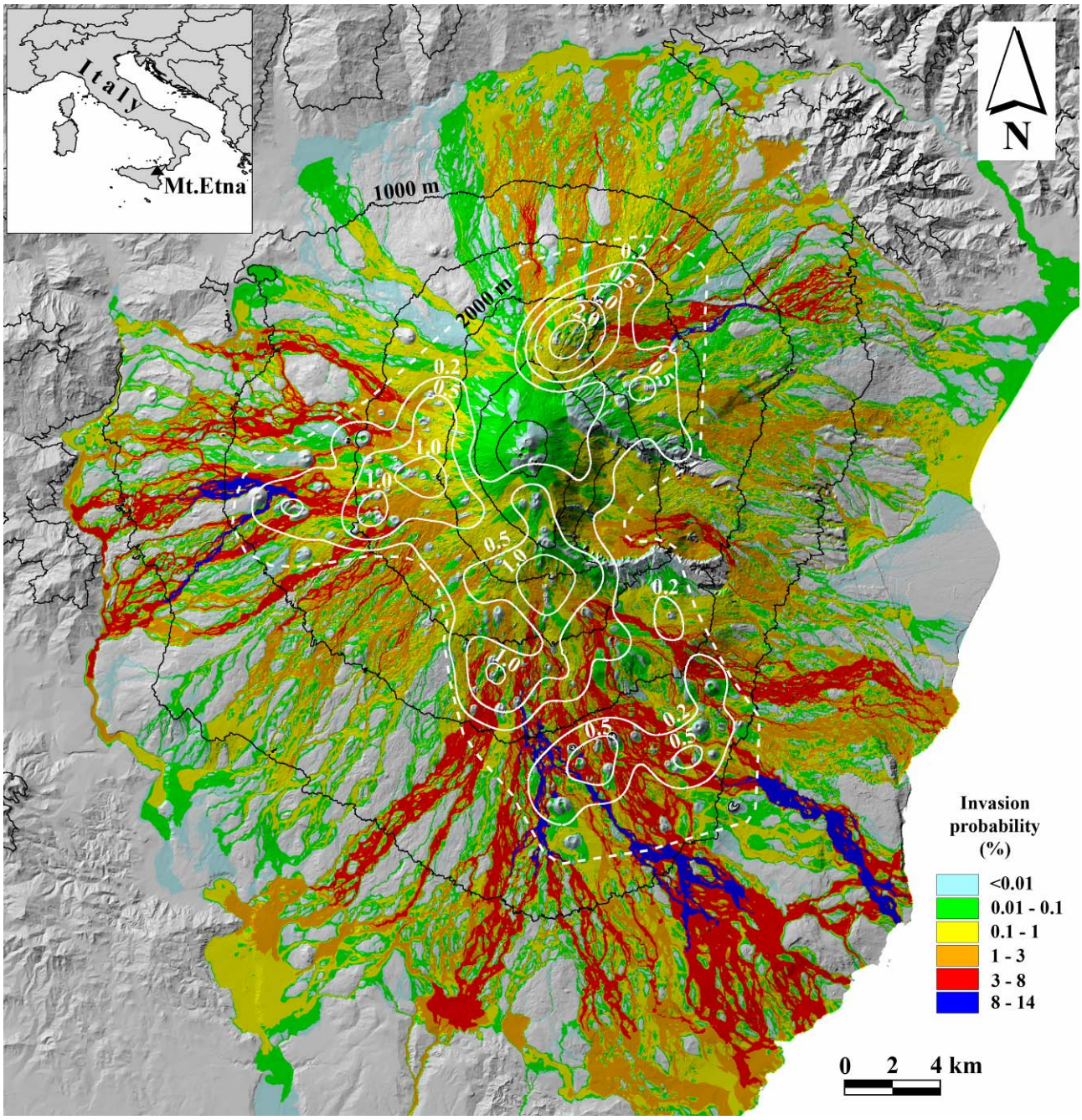

508

509

510 **Fig. 4.** Map of the probability of lava flow inundation of the Mt. Etna area by flank eruptions
511 sourced according to the observed density of vent occurrences. SC: summit craters; VDB: Valle del
512 Bove. White lines are the contours of the probability density of vent formation expressed as % per
513 km^2. The dashed white line delimits the areas in which simulated new-formed vents are located and
514 corresponds to vent opening probabilities higher than 0.1 %/km^2. The inundation probability
515 (equation 2) is expressed as a percentage. Black lines are 500 m contours.

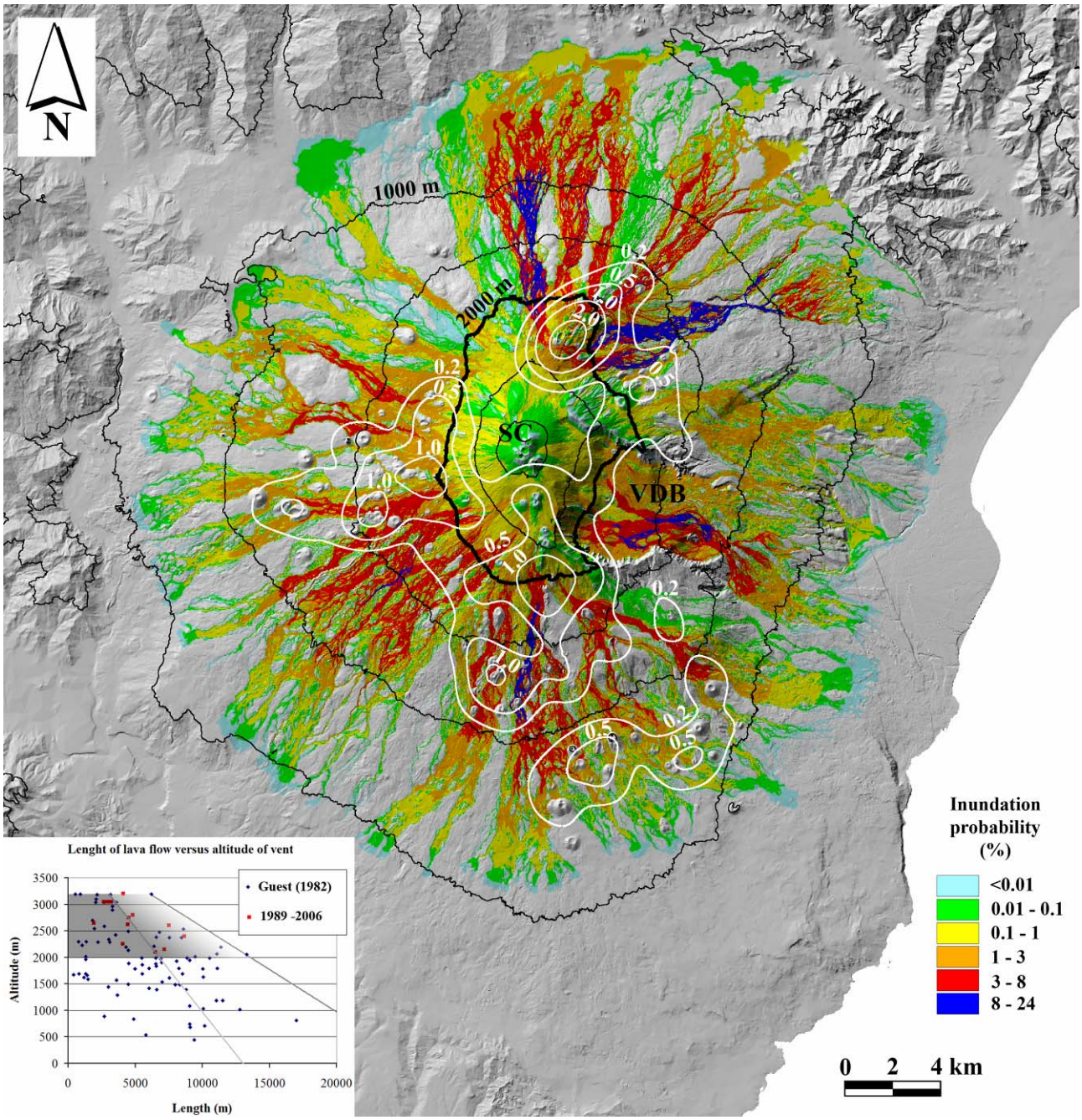

Fig. 5. Map of the probability of lava flow inundation of Mt. Etna from flank vents at elevations above 2000 m (thick black contour). SC: summit craters; VDB: Valle del Bove. White lines are the contours of the probability density of vent formation expressed as % per km^2. The probability of inundation (equation 2) is expressed as a percentage. Black lines represent 500 m elevation

contours. Lower left inset is the plot length vs. altitude of vents; the grey zone represents the elevations and lengths of vents used to create this map.

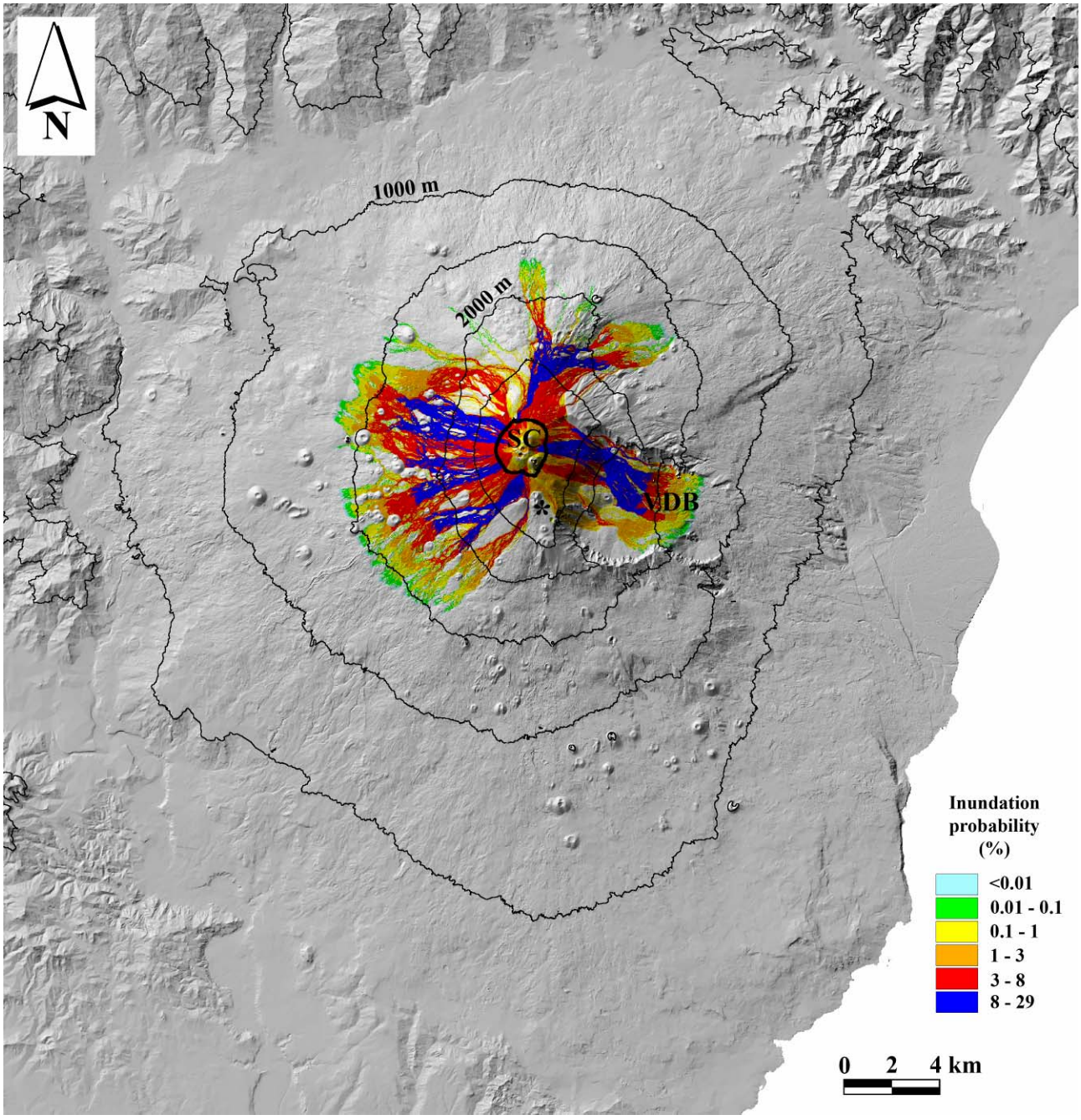

Fig. 6. Map of the probability of lava flow inundation of the Mt. Etna area by new eruptions from vents opened at elevations above 3000 m (calculated using a uniform probability of vent opening). SC: summit craters; VDB: Valle del Bove. The black asterisk indicates the location of the 2002-2003 cones. The inundation probability (equation 2) is expressed as a percentage. Black lines are 500 m elevation contours. The thick black line is the 3000 m contour. The inset highlights the range in elevations and lengths for flows erupted above 3000 m.

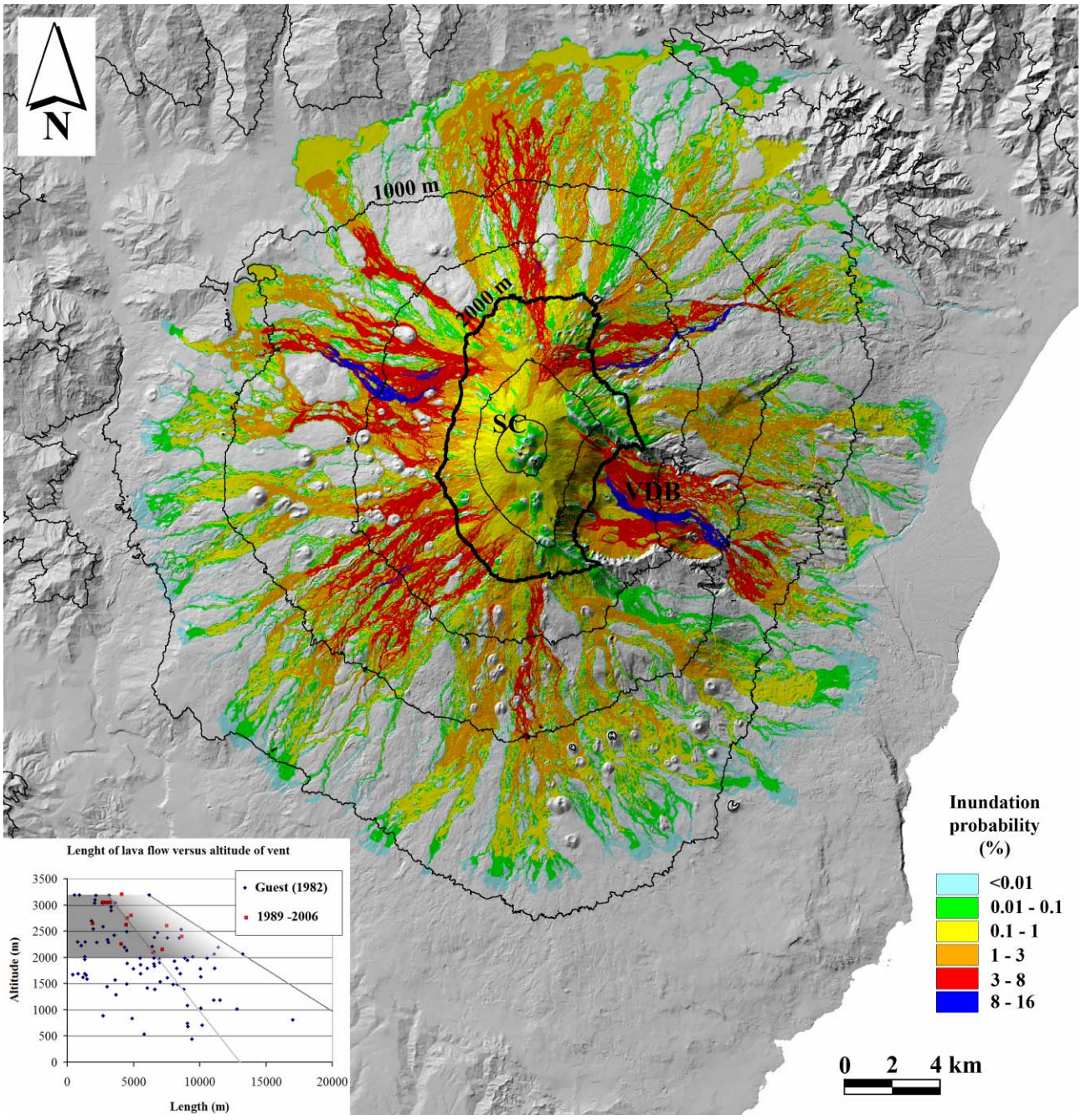

Fig. 7. Map of the probability of lava flow inundation of Mt. Etna from flank vents at elevations above 2000 m (thick black contour) calculated assuming a uniform probability of vent opening. SC: summit craters; VDB: Valle del Bove. The probability of inundation (equation 2) is expressed as a percentage. Black lines represent 500 m elevation contours. The inset highlights the range in elevations and lengths for flows erupted above 2000 m.

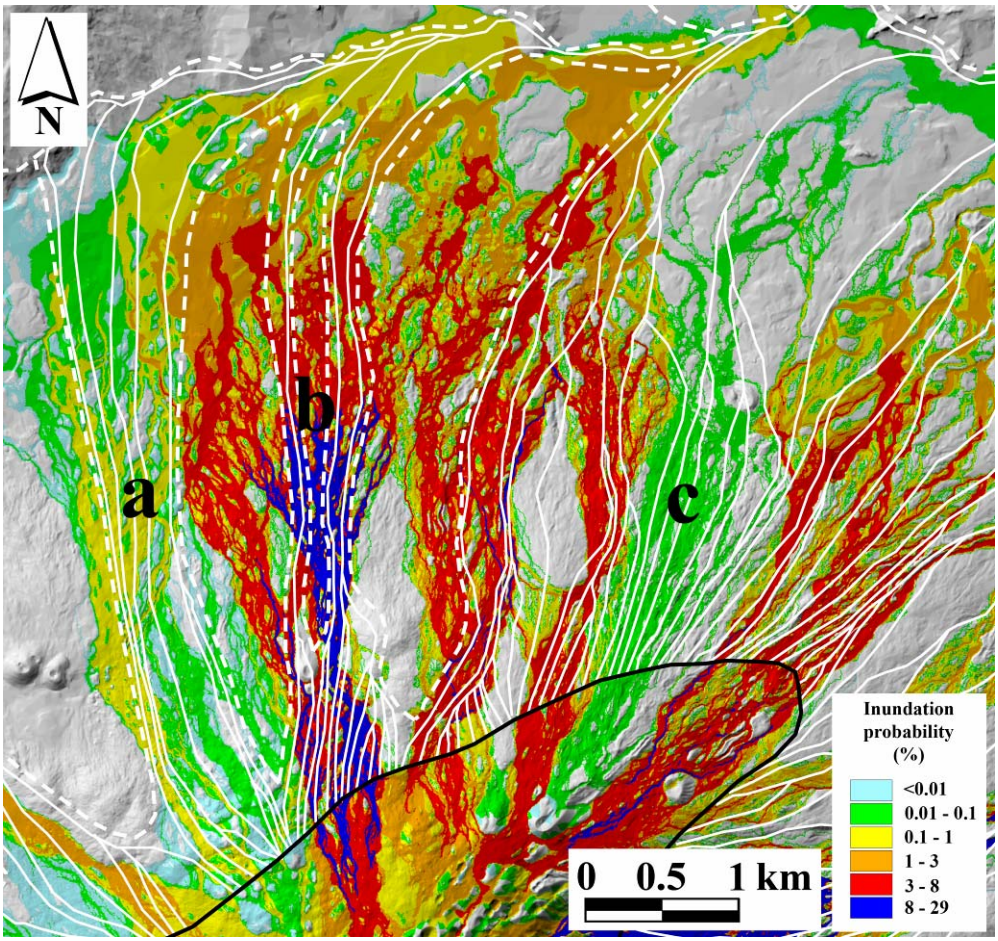

Fig. 8. Comparison between the map of the probability of lava flow inundation of the northern flank of Mt. Etna from flank vents at elevations above 2000 m (Fig. 5) and the possible maximum extent of lava flows (white lines) erupted from the outer edge (black line) of the region with a vent opening probability greater than 1 vent per km^2 (from Fig. 3 of Guest and Murray [1979]).

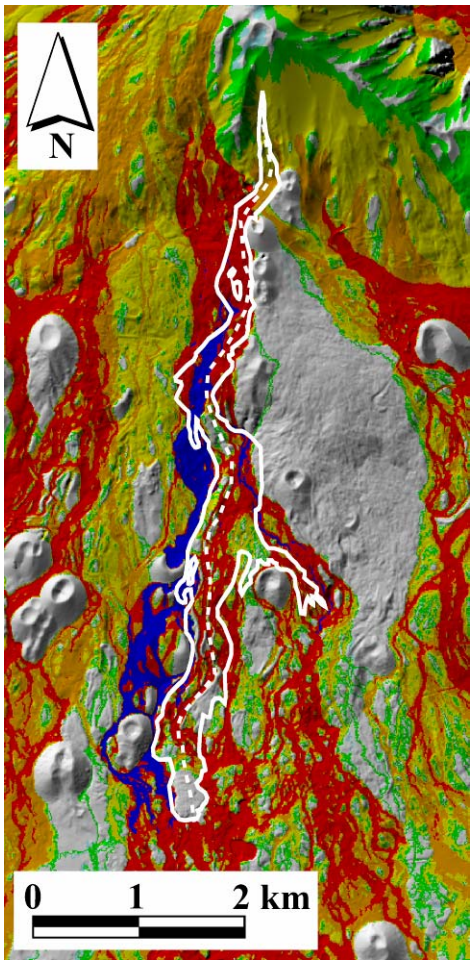

Fig. 9. Effect of the 2001 flow along the southern flank of Mt. Etna (white line; Behncke et al., 2005; Allard et al., 2006) on the map of the probability of lava flow inundation of Mt. Etna (see Fig. 5). The dashed white line is the maximum slope path computed on the 1998 DEM [Tarquini et al., 2007] prior to the emplacement of the 2001 flow. Blue hues represent a high probability of inundation, pale green hues a low probability of inundation (see legend in Fig. 5). The highest probability of inundation occurs along a nearly N-S strip parallel to the 2001 flow. The 2001 flow has zones which may be invaded and others (e.g. its front) that have a very low to zero probability of inundation.

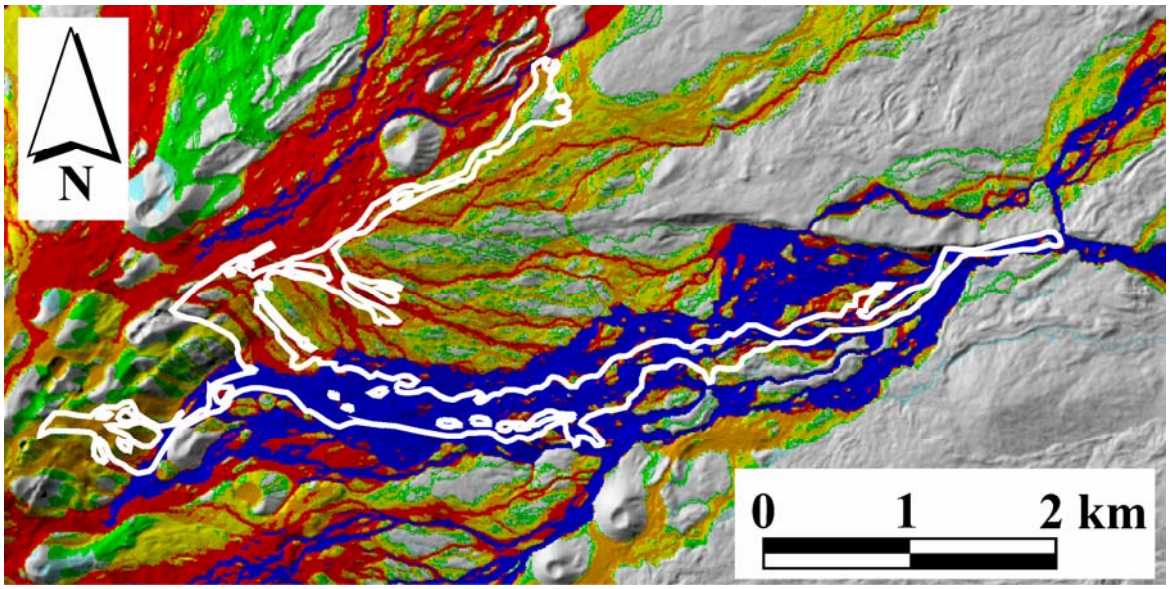

Fig. 10. Effect of the 2002-2003 flow in the northeastern sector of the volcano (white line; Behncke et al., 2005; Allard et al., 2006) on the map of the probability of lava flow inundation of Mt. Etna (see Fig. 5). Blue hues represent a high probability of inundation, pale green hues a low probability of inundation (see legend in Fig. 5). The nearly E-W trending valley, along which the main portion of the 2002-2003 lava flow was emplaced, corresponds to zones with high probabilities of inundation, indicating that future lava flows will likely invade these areas. Other portions, such as the NE-trending branch, show low to very low probabilities of inundation.

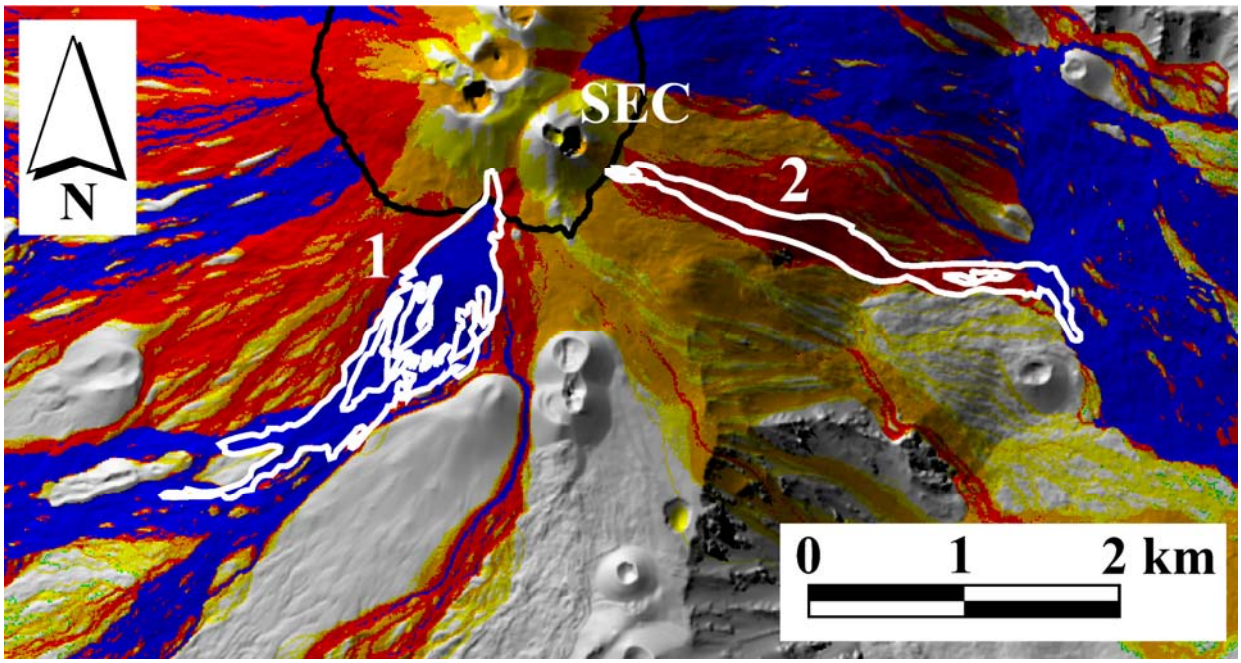

564

565

566 **Fig. 11.** Comparison of lava flows erupted in the Mt. Etna summit area during July/November 2006
567 (white lines; see http://www.ct.ingv.it/Etna2006/MainEng.htm) with the lava inundation map for
568 flows erupted in the summit area (above an elevation of 3000 m; Fig. 6) using a high resolution
569 DEM updated to 2005: 1) southwest lava flows erupted from a vent at an elevation of 3050 m in
570 the period October 27 – November 27, 2006; 2) east lava flow erupted from the southeast crater on
571 July 21, 2006.

572

573

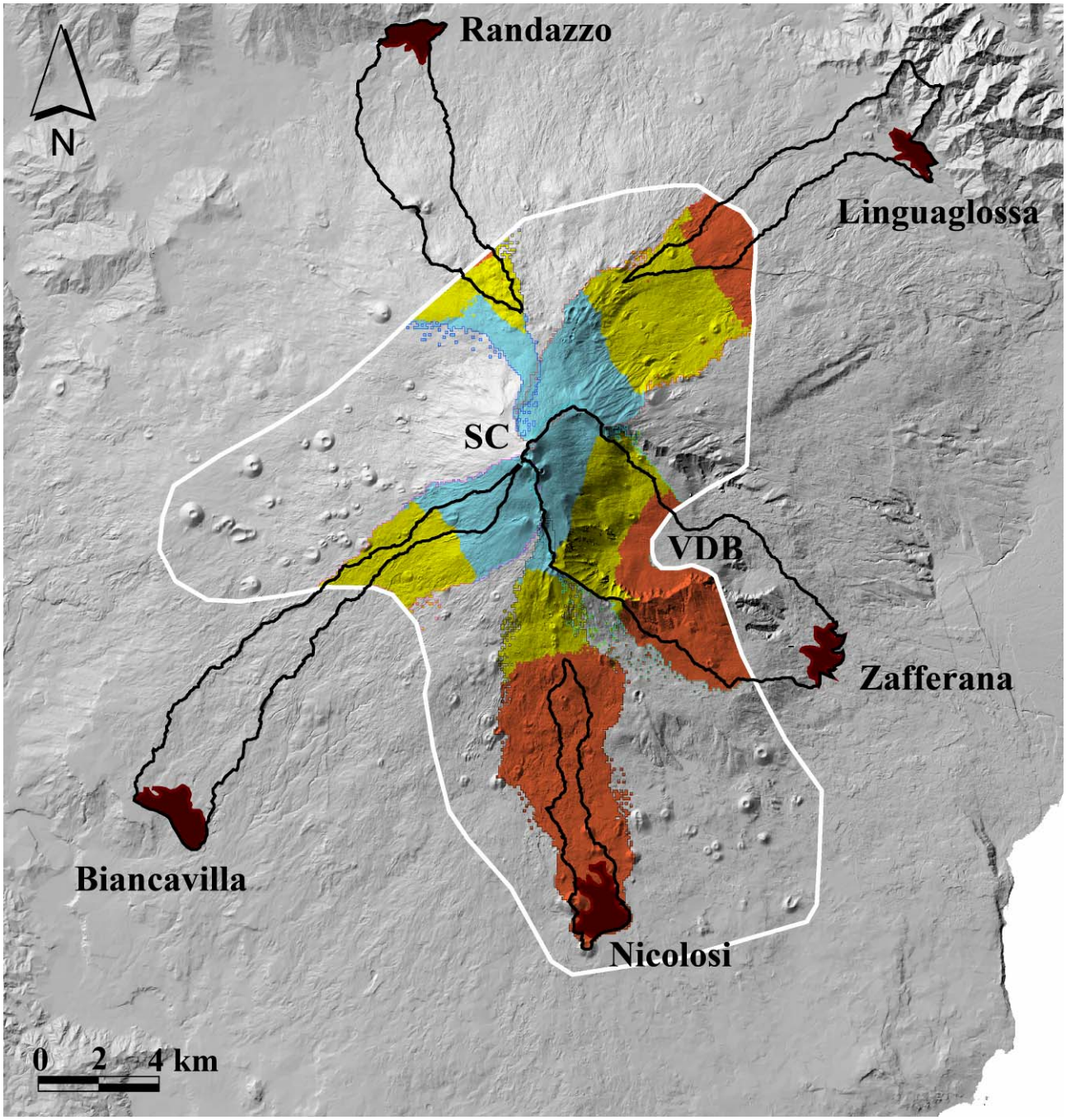

574

575

576 **Fig. 12.** Map of volcano sectors likely to generate lava flows which may invade selected villages at
577 the foot of Mt. Etna. SC: summit craters; VDB: Valle del Bove. Lava erupted from new vents in the
578 colored zones may invade the villages. The thick white line delimits the area in which simulated
579 new-formed vents are located; this area is defined on the basis of the spatial distribution of vents.

Black lines are the hydrological catchment areas for each village. The color code of the lava catchment subdivision refers to that used in figure 3: orange hues represent zones in which the distance between the village and the vents is $\leq 0.5L_l$; yellow hues are zones in which the distance between the village and the vents is $0.5L_l < L_{ij} < L_l$; cyan hues represent zones in which the distance between the village and the vents is $\geq L_l$. According to the adopted model, lava flows from vents in the cyan zones cannot reach the villages.